Research Square

Preprints are preliminary reports that have not undergone peer review.
They should not be considered conclusive, used to inform clinical practice,
or referenced by the media as validated information.

Effects of Bamboo and Cocopeat-Based Cellulose Fibers on the Properties of Low-Carbon Mortar Containing Recycled Brick Aggregates

Steve W.M Supit

stevesupit@polimdo.ac.id

Manado State Polytechnic

Henry F. Aritonang

Sam Ratulangi University

Priyono Priyono

Manado State Polytechnic

Debby Willar

Manado State Polytechnic

Stefani S. Peginusa

Manado State Polytechnic

Research Article

Keywords: recycled brick aggregate, bamboo cellulose fiber, coco peat fiber, pozzolan mortar, compressive strength, flexural strength, low-carbon construction materials

Posted Date: November 18th, 2026

DOI: https://doi.org/10.21203/rs.3.rs-11576517/v1

License: This work is licensed under a Creative Commons Attribution 4.0 International License.
Read Full License

Additional Declarations: No competing interests reported.

Effects of Bamboo and Cocopeat-Based Cellulose Fibers on the Properties of Low-Carbon Mortar Containing Recycled Brick Aggregates

Steve W.M Supit[1*], Henry F. Aritonang[2], Priyono[3], Debby Willar[4], Stefani S. Peginusa[5]

[1,4,5]Civil Engineering Department, Manado State Polytechnic, Indonesia 95252
[2]Faculty of Mathematics and Natural Sciences, Sam Ratulangi University, Indonesia 95115
[3]Mechanical Engineering Department, Manado State Polytechnic, Indonesia 95252
*corresponding author: stevesupit@polimdo.ac.id

Abstract

This study investigates a low-carbon mortar in which 60% of the Portland composite cement (PCC) was replaced by fly ash (40%), limestone powder (15%), and metakaolin (5%), reinforced with alkali-treated bamboo cellulose (CB) or cocopeat cellulose (CCP), and containing recycled brick aggregate (RA) as a 20% replacement for natural sand. First, the CB dosage was varied from 0.5% to 2% of binder mass in plain cement mortar; 1.5% gave the highest 28-day compressive strength (29.9 MPa versus 25.3 MPa for the control) and was adopted for the second stage. Compressive (7 and 28 days) and flexural (28 days) strengths were measured, and hydration and microstructure were examined by X-ray diffraction (XRD) and scanning electron microscopy with energy-dispersive spectroscopy (SEM-EDS). The pozzolanic binder and the cellulose reduced the 7-day compressive strength by up to 32%. XRD indicated that both celluloses retarded early clinker hydration but promoted carboaluminate formation by 28 days, when the fiber mixtures reached 17.2–17.4 MPa, versus 16.6 MPa for the plain pozzolan mortar and 20.0 MPa for the control. The fiber mixtures containing RA reached 20.0–20.1 MPa. Bamboo cellulose gave the highest flexural strength, 5.61 MPa, 31% above the control and 14% above the plain pozzolan mortar, and SEM showed intact bamboo fibers bridging pores, whereas cocopeat cellulose left it practically unchanged (4.98 versus 4.90 MPa). The load–displacement curves showed that bamboo cellulose raised both the peak load and the displacement at failure of the pozzolan mortar, consistent with microcrack bridging, although no mixture showed a post-peak softening branch. RA reduced the flexural strength of the bamboo and cocopeat mixtures by 33% and 28%, to 3.78 and 3.59 MPa, respectively, below that of the control. The bamboo cellulose mortar with RA therefore offers the best balance of clinker reduction, waste valorization, and strength, with flexural performance as the main limitation.

Keywords: *recycled brick aggregate; bamboo cellulose fiber; coco peat fiber; pozzolan mortar; compressive strength; flexural strength; low-carbon construction materials*

1. Introduction

The worldwide construction industry is under increasing pressure to become more environmentally friendly. Cement production is responsible for about 7-8% of all global CO_2 emissions, mainly because of the energy-intensive production of clinker and the calcination of limestone. This has resulted in a rapid expansion of research into low-carbon mortar and concrete, with strategies being pursued to reduce embodied carbon while maintaining the mechanical performance required for structural and masonry applications. Low carbon mortar is not a different material but an improvement of standard cementitious systems that can be achieved by reducing the clinker content and using partial replacement of supplementary cementitious materials, recycled aggregates, and renewable reinforcing materials while maintaining similar strength, durability, and workability.

Among the available strategies, the use of recycled construction and demolition waste as aggregate has been the focus of particular attention for its ability to reduce carbon emissions and divert waste from landfills. Recycled aggregate concrete (RAC) has the potential to reduce landfill disposal significantly while reducing dependence on virgin materials. However, the mechanical and durability performance of RAC is often regarded as inferior to that of conventional concrete because of the inherent properties of recycled aggregates, although it offers environmental advantages.

Quantitative studies consistently report that the incorporation of recycled aggregates leads to reductions in mechanical properties. The reduction in the compressive strength of RAC is generally in the range of 5-25% for high replacement levels (50-100%) (Islam et al., 2025). Some other studies show larger reductions of up to 15-30%, based on the quality of the aggregate and mix design (Zhang et al., 2022). More detailed experimental studies indicate that even moderate replacement levels (25-50%) can lead to strength loss of the order of 10-30% compared to natural aggregate concrete. In addition, tensile strength and flexural strength are negatively impacted, with a generally 6%–20% reduction when the replacement ratio increases. Even after long-term curing periods, residual differences of about 5–10% can still be observed (Xiao et al., 2026). However, the long-term strength development may partially compensate for the early-age reductions. The

porous and heterogeneous nature of recycled aggregates inherently causes such reductions. Recycled aggregates generally have much higher water absorption (up to 8%) than natural aggregates (around 1–3%) due to the presence of adhered old mortar. This results in higher porosity of RAC, which has been reported to increase by 40% to over 100% compared to that of conventional concrete, depending on the replacement ratio. In extreme cases, full replacement (100% RA) can cause porosity increases of over 125% and a significant degradation of the interfacial transition zone (ITZ) (Wang et al., 2025). This trend is especially relevant for recycled clay-brick aggregates, whose interfacial transition zone is more porous and weaker than that of the recycled concrete aggregate, which contributes to strength loss (Chang et al., 2022). These microstructural deficiencies are responsible for higher permeability, lower stiffness, and reduced resistance to durability-related degradation mechanisms. Despite these limitations, several strategies have been proposed to enhance RAC performance, including mechanical and chemical pre-treatment of aggregates, incorporation of supplementary cementitious materials, and optimization of mix design parameters.

In this regard, fiber reinforcement has gained attention as an effective method to improve crack resistance and toughness. However, conventional fibers such as steel and synthetic polymers may compromise sustainability due to their high embodied energy and environmental impact. Recently, cellulose-based fibers, particularly micro- and nano-scale cellulose, have emerged as a promising bio-based alternative. Owing to their high aspect ratio, large specific surface area, and intrinsic mechanical strength, cellulose nanofibers (CNF) and nanocrystals (CNC) can enhance cement hydration, refine pore structure, and improve the ITZ at the nano-scale (Allujami et al., 2022; Raghunath et al., 2023; Zormati et al., 2023). At the fiber scale, alkali-treated natural lignocellulosic fibers such as bamboo and coconut coir have similarly been shown to improve flexural strength and crack-bridging behavior in cement mortars at optimized dosages, although excessive fiber content or poor dispersion can offset these gains through agglomeration and increased porosity (Ahmad et al., 2022; Pederneiras et al., 2021; Sanchez-Echeverri et al., 2020; Vagestan et al., 2025).

Nevertheless, the use of cellulose fibers in low-carbon mortar containing RAC systems is still limited and not well understood. The available research studies in the literature mainly consider the recycled aggregates and the cellulose reinforcement as independent modifications, with few studies on the combined or synergistic effects. In particular, the systematic understanding of the

ways in which cellulose fibers can compensate for the inherent increased porosity (up to >100%) and strength loss (up to 30%) of RAC is still lacking. Also, issues of fiber dispersion, optimal dosage, and long-term durability performance are yet to be solved (Wei et al., 2022). Even when fiber reinforcement and recycled aggregates have been combined in one single mixture, most of these studies have focused on a recycled concrete aggregate, not a recycled clay-brick aggregate, and have not decoupled the effect of the cellulose type on the resulting compressive-flexural trade-off (Xu et al., 2024; Ferrández et al., 2024). Thus, this study aims to bridge these gaps by investigating the incorporation of cellulose fibers as a reinforcing strategy in low-carbon mortar made with recycled aggregates. The novelty of this research is to develop an optimized and sustainable mortar system with a low carbon footprint, which improves at the same time the mechanical performance. This contributes to the progress of high-performance RAC as a material applicable to sustainable and circular construction practices. A successful strategy for reinforcing cellulose fibers could be useful in recovering the mechanical performance lost through the substitution of recycled aggregates while further reducing the embodied carbon and waste footprint of the resulting mortar.

2. Materials

The mortar mixtures investigated in this study were formulated from the constituent materials, i.e., Portland Composite Cement, fly ash and limestone powder, metakaolin (after calcination of raw kaolin at 800℃ for 6 hours), and recycled brick aggregate (RA) obtained from construction and demolition waste and used as a partial replacement for natural fine aggregate in selected mixtures. The recycled brick aggregate was crushed using the grinding machine and passed the No.4 sieve. The raw materials of cellulose fibers and recycled brick aggregate can be seen in Figure 1. The chemical composition of the main materials used in this experiment is presented in Table 1.

Bamboo cellulose (CB) and coco peat cellulose (CCP) fibers, extracted from raw bamboo and cocopeat and subjected to alkaline (NaOH) and acid (HCl) treatment as described in Section 3.1, are used as the bio-based reinforcing fibers. Superplasticizer-type Sikacim Concrete from Sika Company was used to maintain adequate workability given the water demand of the fibers and recycled aggregate. The morphology of cellulose bamboo and cellulose cocopeat was analyzed using scanning electron microscopy using 200x and 1000x magnification, as seen in Figure 2. The

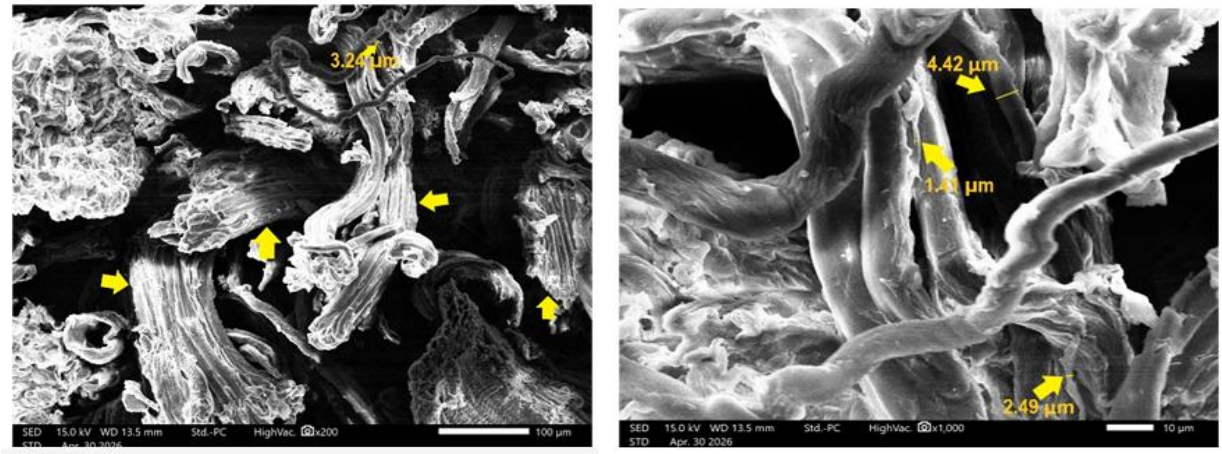
cellulose bamboo surface exhibits a compact and dense structure with particles of varying shapes and sizes. Among these heterogeneous particles, fiber bundles are observed to aggregate into larger lignocellulosic matrix structures. The rough and irregular fiber surfaces consist of amorphous components, including pectin, lignin, hemicellulose, cellulose, and other impurities (Razali et al., 2022). Bamboo cellulose fibers exhibited an average diameter of 3.40 µm and a lower standard deviation of 1.18. The particle surfaces are observed to be highly rough and irregular, where the cellulose component remains strongly enclosed by protective amorphous matrices such as pectin, lignin, hemicellulose, and various impurities (Razali et al., 2022). In this experiment, the percent of hemicellulose, cellulose, and lignin of cellulose bamboo was 16.5%, 40.25%, and 21.68%, respectively.



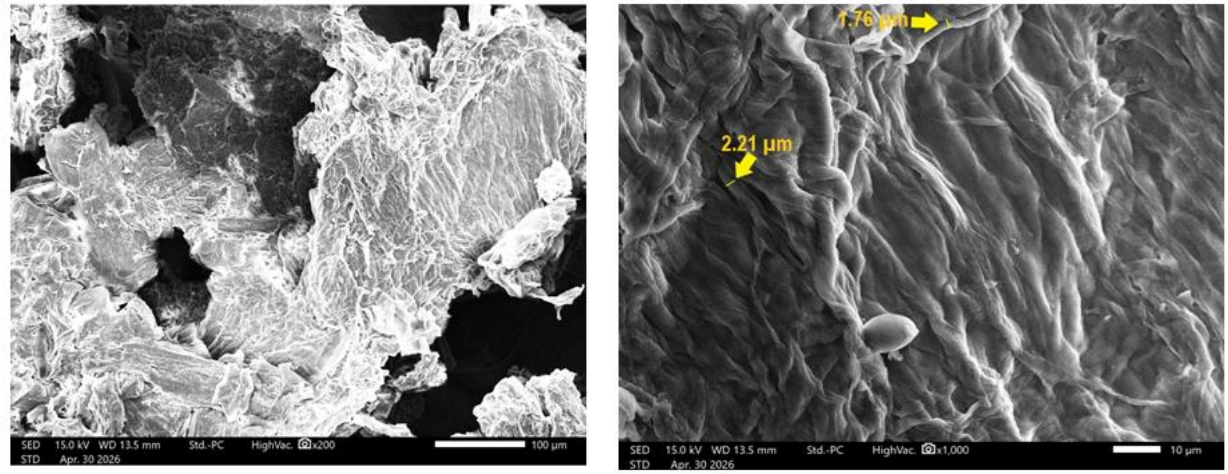
(a) Bamboo fiber (b) Cocopeat fiber (c) Brick waste aggregate

Figure 1. Raw cellulose fibers and recycled brick aggregate

In cellulose extracted from cocopeat, a structural transformation is observed in which the folded and hollow solid fibers become softer and more elongated, without the folds and cavities previously present. The fiber diameter was found to be about 1.76 to 2.26 µm for fibers with clearly distinguishable boundaries and around 900 nm in size based on particle size analysis. Measurements were performed only on fibers with clearly visible edges separating them from adjacent fibers; however, the overall fiber diameter distribution could not be determined because most of the material underwent agglomeration. In this experiment the amount of cellulose was found to be 23% hemicellulose, 22.29% cellulose, and 35% lignin. The percentage of cellulose can be seen higher in bamboo fiber compared to cocopeat fiber.



(a) Morphology of cellulose bamboo



(b) Morphology of cellulose cocopeat

Figure 2. Morphology of (a) cellulose bamboo and (b) cellulose cocopeat

Table 1. Chemical composition of main materials in percent

Oxide Component	Cement (PCC)	Metakaolin	Fly Ash	Limestone
SiO_2	20.92	43.88	18.77	-
Al_2O_3	5.49	38.79	6.89	-
Fe_2O_3	3.78	0.42	21.8	0.51
MgO	0.97	0.92	4.65	-
CaO	65.21	0.91	28.13	99.1

Na_2O	-	0.23	7.41	-
K_2O	-	0.73	1.38	-

3. Experimental Methods

3.1 Preparation of Alkali-Treated Cellulose Fibers from Bamboo and Coco Peat

The first step involved preparing a 20% sodium hydroxide (NaOH) solution. A total of 200 g of NaOH was weighed using an analytical balance and dissolved in 600 mL of distilled water while continuously stirred until completely dissolved. Distilled water was then gradually added until the total solution volume reached 1000 mL, producing a homogeneous solution. Subsequently, a 2% hydrochloric acid (HCl) solution was prepared by diluting 23.7 mL of concentrated HCl (approximately 37%) with distilled water to a final volume of 1000 mL. The dilution process was carried out in a well-ventilated area to minimize exposure to acidic fumes.

The next stage involved the alkalization treatment of the fibers. A total of 1000 g of cleaned bamboo fibers and 1000 g of cleaned coco peat fibers were separately placed in heat-resistant containers. Subsequently, 2000 mL of 20% NaOH solution was added to each container until the fibers were completely submerged. The mixtures were heated on a hot plate at approximately 80–100°C for 3 hours, with periodic stirring to ensure uniform treatment. During heating, the fibers gradually turned dark brown, indicating the dissolution of lignin and hemicellulose components. After treatment and cooling, the fibers were separated from the solution using a No. 200 sieve and repeatedly washed with distilled water until the rinse water reached a pH of approximately 10.

The subsequent stage was neutralization using 2% HCl solution. The alkali-treated fibers were immersed in 1000 mL of 2% HCl solution for 1 hour in a closed container to neutralize any residual alkaline solution on the fiber surfaces. After neutralization, the fibers were washed again with distilled water until a neutral pH (pH 7) was achieved, ensuring that no acidic or alkaline residues remained.

The final stage consisted of drying the cellulose fibers in an oven at 60°C for approximately 24 hours to reduce moisture content. The dried cellulose fibers were then ready for use as reinforcing materials in the mortar mixtures. This sequential alkalization–neutralization protocol follows treatment approaches widely reported to remove non-cellulosic surface constituents (lignin,

hemicellulose, waxes) from lignocellulosic fibers, thereby roughening the fiber surface and improving fiber–matrix bonding in cementitious composites (Sanchez-Echeverri et al., 2020; Vagestan et al., 2025).

3.2 Mixture Proportions

In order to investigate the maximum percentage of fiber that can be used as an additive in pozzolan mortar containing recycled aggregate as a replacement of sand, the effect of fibers on compressive strength development in cement mortar by using cellulose bamboo with a variation of percentage, i.e., 0.5%, 1%, 1.5%, and 2% by weight of binder (cement only in stage one), was evaluated (stage one). The percentage that gave the highest contribution of compression load resistance in this case, 1.5% dosage, was then selected to evaluate the influence of using cellulose bamboo and cellulose cocopeat when used as an additive in pozzolan mortar containing recycled aggregate (stage two). The mixture proportions of mortar that were used in stage two can be seen in Table 2.

Table 2. Mixture proportion of variations of mortar in stage two (kg/m³)

No	Mix Code	Unit: kg/m³								
		Cement	Fly Ash	Limestone	Metakaolin	Cellulose Fiber	Fine Aggregate	RA	Water	SP
1	MC	500	0	0	0	0	1000	0	200	2.5
2	PM	200	200	75	25	0	1000	0	200	2.5
3	PM-CB1.5%	200	200	75	25	7.5	1000	0	200	2.5
4	PM-CCP1.5%	200	200	75	25	7.5	1000	0	200	2.5
5	PM-CB1.5%-RA	200	200	75	25	7.5	800	200	200	2.5
6	PM-CCP1.5%-RA	200	200	75	25	7.5	800	200	200	2.5

Note: MC = control mortar; PM = pozzolan mortar; CB = bamboo cellulose fiber; CCP = coco peat cellulose fiber; RA = recycled brick aggregate; SP = superplasticizer

The entire set of tools and materials required for the preparation of the mortar test specimens was collected together and weighed out according to the planned mix design. The specimen molds were cleaned and lightly coated with oil to facilitate demolding when the mortar hardened. In stage two, the binding materials (cement, fly ash, limestone powder, and metakaolin) were introduced to the

mixing container and mixed evenly. Natural fine aggregates and recycled brick aggregate were added to the container according to the intended mix variation and were mixed until the dry materials formed a homogeneous blend. Then, bamboo cellulose or coco peat fibers were added gradually and mixed slowly to obtain a uniform dispersion without clumping. The water was added gradually while mixing with a mechanical mixer until the mortar reached the suitable consistency. Superplasticizer was used to improve workability. The fresh mortar was poured in layers into the molds, and each layer was compacted with an iron tamper to remove air voids. The surface was finally leveled with a trowel. The specimens were allowed to set in their molds until adequately cured. The specimens were removed from the molds and labeled according to their respective mix variations. The specimens were cured to the intended testing age.

3.3 Compressive Strength Test

The compressive strength of the mortar specimens was measured following ASTM C109, "Standard Test Method for Compressive Strength of Hydraulic Cement Mortars (Using 2-in. or [50-mm] Cube Specimens)." Mortar cubes of 50 mm × 50 mm × 50 mm were prepared in stainless steel molds and compacted in two layers to reduce the entrapment of air voids and finished with a flat trowel. After 24 ± 2 h, the specimens were removed from the molds and cured in a water tank at 23 ± 2°C until testing ages of 7 and 28 days. The specimens were removed from the curing tank and surface dried before testing, and the bearing surfaces were checked for flatness and cleanliness to ensure uniform load distribution. Each cube was placed centrally on the lower platen of a compression testing machine, with the cast faces in contact with the platens. The load was applied continuously at a controlled rate until failure. The maximum load at failure was recorded, and the compressive strength was calculated by dividing the failure load by the cross-sectional area of the cube (2500 mm^2). Three specimens were tested for each mix and curing age, and the average value was reported as the representative compressive strength. The results that deviate markedly from the mean were discarded in accordance with ASTM C109 outlier provisions.

3.4 Flexural Strength Test

The flexural strength of the mortar was evaluated following ASTM C348, "Standard Test Method for Flexural Strength of Hydraulic Cement Mortars." Prismatic specimens with dimensions of 40 mm × 40 mm × 160 mm were cast in accordance with the mix proportions used for the compressive specimens, compacted to eliminate entrapped air, and finished with a flat trowel to obtain a

uniform top surface. After demolding at 24 ± 2 h, the prisms were cured in a water bath at 23 ± 2°C until the testing age of 28 days. At the time of testing, each specimen was removed from the curing tank, surface-dried, and placed in the flexural testing apparatus using the simple-beam (three-point loading) configuration, with the specimen supported on two lower rollers spaced at a span of 120 mm and the load applied centrally through a single upper roller. The load was applied in small increments without shock until fracture occurred, the mid-span displacement was read at intervals of about 0.01 mm to obtain the load–displacement curves (Section 4.2.3), and the maximum load at failure was recorded. The flexural strength (modulus of rupture) was then calculated using the standard flexural formula for a rectangular cross-section under three-point loading, $R = 3PL/2bd^2$, where P is the maximum applied load, L is the span length, and b and d are the width and depth of the specimen, respectively. Three specimens were tested for each mix, and the average flexural strength was reported, following the same outlier-exclusion criteria specified in the corresponding ASTM standard.

3.5 Scanning Electron Microscopy

The microstructure was examined on paste specimens of MC, PM, PM-CB 1.5%, and PM-CCP 1.5% after 28 days of curing. The dried fragments were mounted on aluminum stubs with conductive carbon tape and sputter-coated with gold to prevent charging. Images were acquired in secondary electron (SE) mode on a JSM-7800F at an accelerating voltage of 15-20 kV, and the elemental composition was measured with an energy-dispersive X-ray spectroscopy (EDS) detector at five spots per micrograph (Spectra 1–5). In this case, one spot was selected as a representative. Weight percentages were converted to atomic Ca/Si and Al/Si ratios. Because the fracture surfaces are rough and the EDS interaction volume (a few micrometers) can include more than one phase, the analyses were treated as semi-quantitative and were used to identify the dominant phase at each spot rather than to determine the composition of the C-S-H gel; carbon contents are indicative only because of the carbon tape and possible surface carbonation (Scrivener et al., 2016).

3.6 X-Ray Diffraction

Phase changes during hydration were examined by X-ray diffraction (XRD) on paste samples of MC, PM, PM-CB1.5% and PM-CCP1.5% after 7 and 28 days of curing. Patterns were recorded

on a Rigaku D/Max diffractometer with Cu Kα radiation (λ = 1.5406 Å) at 40 kV and 30 mA over 10–70° 2θ with a step size of 0.02°. Crystalline phases were identified by matching peak positions to the DIFFRAC. EVA and ICDD PDF-5+ reference database using TOPAS v.6 software.

4. Results and Discussion

4.1 Effect of Bamboo Cellulose Fiber on Compressive Strength of Mortar (Stage 1)

Figure 3 shows the compressive strength results, demonstrating the influence of adding bamboo cellulose (CB) at 0.5%, 1%, 1.5%, and 2% by weight of total binder (500 kg/m³) on the mechanical properties of the mortar compared to the cement-only control mortar without fiber (NM) at 7 and 28 days of curing. The reference was the control mortar (NM), which showed compressive strengths of 21.4 MPa and 25.3 MPa at 7 and 28 days, respectively. At a low dosage of 0.5% (CB0.5%), the compressive strength slightly decreased to 19.3 MPa (7 days) and 23.8 MPa (28 days), implying that a small addition of bamboo cellulose fiber may have introduced minor voids or interfered marginally with cement hydration and packing density, without providing sufficient reinforcing benefit at this stage. At 1% (CB1%), the compressive strength recovered to values close to the control, reaching 21.6 MPa and 24.6 MPa at 7 and 28 days, respectively, indicating that at this concentration the fiber started to contribute positively to the microstructure, probably due to improved fiber-matrix bonding or crack-bridging effects that counteracted the dilution effect of the cement.

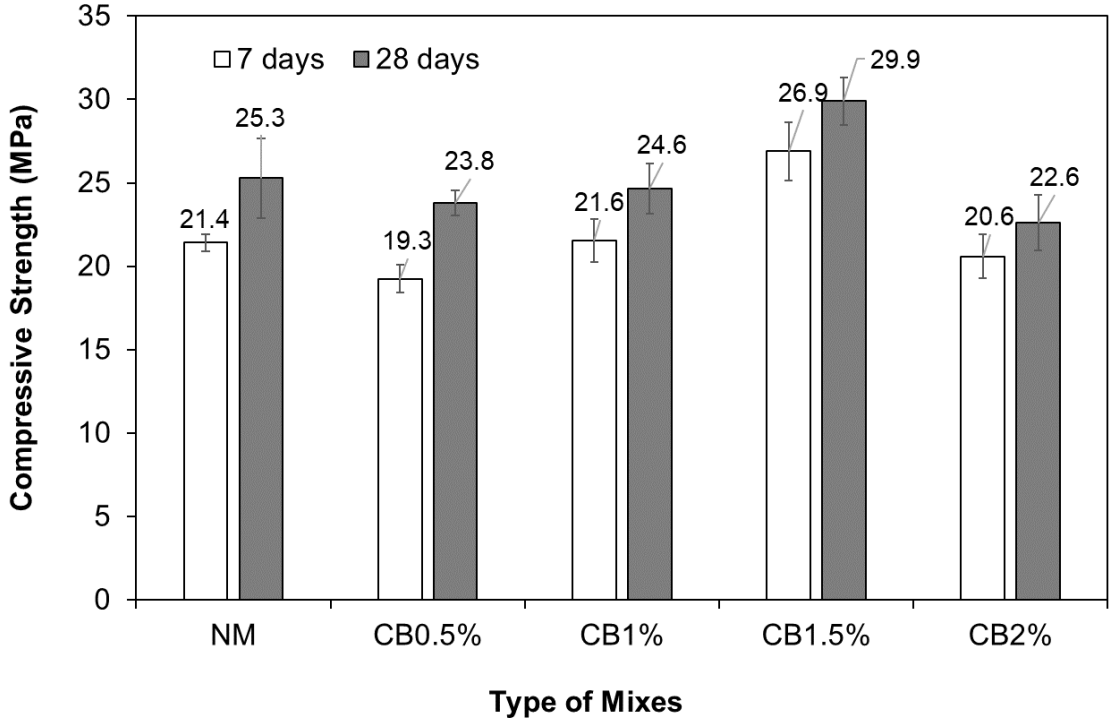


Figure 3. Effect of bamboo cellulose (CB) fiber dosage on the compressive strength of mortar at 7 and 28 days.

The most notable enhancement was observed at 1.5% dosage (CB1.5%), where the compressive strength increased substantially to 26.9 MPa at 7 days and 29.9 MPa at 28 days, representing the highest values among all mixtures and a marked improvement over the control mortar. This significant increase suggests that at this optimum dosage the bamboo cellulose fibers were well-dispersed within the cementitious matrix, effectively bridging microcracks, restraining crack propagation, and enhancing the internal cohesion of the hydration products, likely due to a synergistic interaction between the fiber's mechanical reinforcement and possible pozzolanic or filler effects that refined the pore structure. However, beyond this optimum point, at a 2% dosage (CB2%), the compressive strength declined to 20.6 MPa and 22.6 MPa at 7 and 28 days, falling below even the control mortar values. This reduction is consistent with the fiber agglomeration or clustering commonly reported at higher dosages in bamboo- and coir-fiber reinforced cementitious composites, where non-uniform dispersion, increased porosity, and weaker interfacial zones progressively offset the reinforcing benefit and reduce overall matrix density (Sanchez-Echeverri et al., 2020; Sekar & Kandasamy, 2018; Vagestan et al., 2025). Overall, the results indicate that 1.5% bamboo cellulose content represents the optimum dosage for maximizing compressive

strength, beyond which the addition becomes detrimental, likely due to workability and dispersion issues associated with excessive fiber content, while the consistent trend of increasing strength from 7 to 28 days across all mixtures reflects the ongoing hydration and pozzolanic reactions contributing to strength development over time. Fu et al. (2025) similarly reported that raw bamboo fiber-reinforced phosphogypsum-based composites reached maximum compressive and flexural strengths at an intermediate fiber length and content, beyond which performance declined, and attributed the decline to reduced fiber–matrix contact and less uniform hydration-product coverage on the fiber surface at higher loadings, an interpretation consistent with the agglomeration-driven decline observed for CB2% in the present study.

4.2 Effect of Bamboo and Coco Peat Cellulose Fiber on Pozzolan Mortar Containing Recycled Brick Aggregate (Stage 2)

4.2.1 Workability

The workability of the fresh mortar was measured with a flow table in accordance with ASTM C1437. The spread diameter was measured along four lines and averaged, and the flow was calculated as the percentage increase over the base diameter. The flow table results of the six mixtures are presented in Figure 4. Because all mixtures had the same water-to-binder ratio (0.40) and superplasticizer content (2.5 kg/m³), the differences in spread reflect the water demand of the constituents directly. The control mortar (MC) showed the highest spread, 185 mm (flow of 82%). Replacing 60% of the cement with fly ash, limestone, and metakaolin reduced the spread of PM to 150 mm (48%), a reduction of about 19%. Although spherical fly ash particles usually improve workability, the fly ash used here is a high-calcium, iron-rich ash (Table 1), and its effect was outweighed by the very high specific surface area and water demand of metakaolin and the fine limestone powder. Together these increase the surface area that must be wetted by the same amount of mixing water.

Adding 1.5% cellulose further reduced the spread to 140 mm for PM-CB1.5% (−7% relative to PM) and 145 mm for PM-CCP1.5% (−3%). Cellulose is hydrophilic: it absorbs part of the free mixing water, and the fibers form an entangled network that restrains the flow of the fresh paste. Bamboo cellulose reduced the workability slightly more than cocopeat cellulose, which is consistent with its more fibrous, higher-aspect-ratio morphology (Section 2): elongated fibers interlock and resist flow more effectively than the largely agglomerated, particle-like cocopeat

cellulose. However, the difference between the two celluloses (5 mm) is small and close to the precision of the test.

Replacing 20% of the natural sand with recycled brick aggregate gave the lowest spreads, 130 mm for PM-CB1.5%-RA and 135 mm for PM-CCP1.5%-RA, about 7% lower than the corresponding mixtures without RA. Crushed clay brick is porous and angular. It absorbs part of the mixing water, and its rough particles increase inter-particle friction, both of which reduce flow (Dang et al., 2018). The water absorbed by the brick aggregate also lowers the effective water-to-binder ratio of the paste, which may explain why the RA mixtures reached the highest compressive strengths of the pozzolan mixtures. The water held in the brick pores could then be released gradually to support continued hydration (internal curing). On the other hand, less free water is available to wet and disperse the fibers. This factor probably contributed to the loss of the flexural benefit of both celluloses in the RA mixtures (Section 4.2.3). In practice, the superplasticizer dosage of the pozzolan, fiber,, and RA mixtures could be increased, or the RA pre-saturated, to restore a workability closer to that of the control mortar.

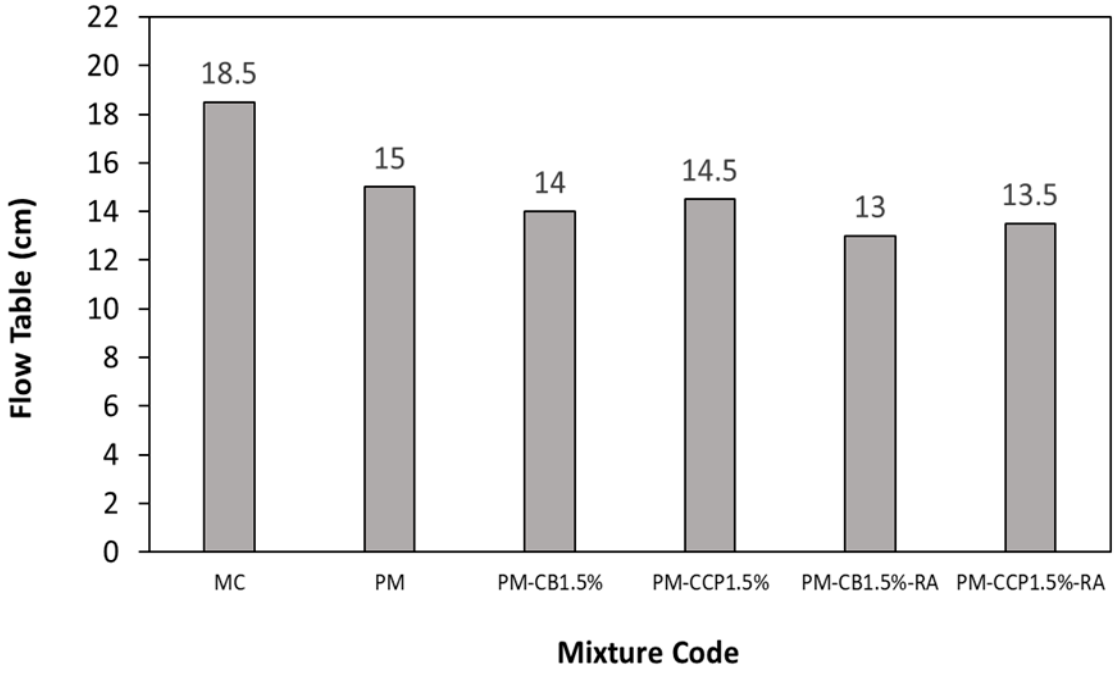


Figure 4. Workability of mortar mixtures based on the flow table test

4.2.2 Compressive strength

Figure 5 presents the compressive strength development of six mortar mixtures at 7 and 28 days. The different batch mixtures include normal mortar (MC), pozzolan mortar (PM), pozzolan mortar reinforced with 1.5% bamboo cellulose (PM-CB1.5%), pozzolan mortar containing 1.5% coco peat cellulose (PM-CCP1.5%), and the corresponding mixtures incorporating recycled brick aggregate (RA) as a replacement for natural fine aggregate. Compared with the control mortar (MC) in this batch, the pozzolan mortar (PM) exhibited a reduction in compressive strength at both curing ages: the 7-day strength decreased from 16.6 MPa (MC) to 14.4 MPa (PM), while the 28-day strength decreased from 20.0 MPa to 16.6 MPa. This reduction can be attributed to the slower pozzolanic reaction, which generally contributes less to early-age strength than ordinary cement hydration, together with the dilution effect caused by partial cement replacement (Xiao et al., 2026).

This behavior can be primarily attributed to the high total replacement level of 60%, which leads to the PCC proportion being 40% and hence to the presence of reactive phases derived from clinker. Fly ash and metakaolin also take part in the strength development by pozzolanic reactions of the secondary type. However, the rate of these reactions is generally lower than the primary hydration of Portland cement. The secondary reaction products, therefore, did not contribute enough at the curing age investigated to compensate for the dilution effect due to the high replacement by fly ash. The 15% limestone may also act as a filler and may be involved in the formation of carboaluminates in the presence of metakaolin. But its role in strength development is not the same as that of PCC. The 5% metakaolin can enhance pozzolanic activity and pore refinement because of its high aluminosilicate reactivity, but its relatively low proportion is not sufficient to totally compensate for the decrease in PCC content caused by the replacement of 40% fly ash and 15% limestone. Therefore, the strength development of the blended binder is a trade-off between cement dilution, fly ash reactivity, pozzolanic reaction caused by metakaolin, effects of limestone filler, and densification of the microstructure. The difference in strength may be less significant at longer curing ages as the pozzolanic reactions of fly ash and metakaolin proceed. The inclusion of 1.5% of bamboo cellulose (CB) in the pozzolan mortar also reduced the 7-day compressive strength to 12.5 MPa, which is about 25% lower than MC. The reduction can be related to the increase of the porosity and water absorption promoted by cellulose fibers, which

may prevent the densification of the matrix. However, the compressive strength increased to 17.4 MPa at 28 days, indicating that the continuing hydration and pozzolanic reactions partially compensated for the initial strength loss, but the strength was lower than the control mortar.

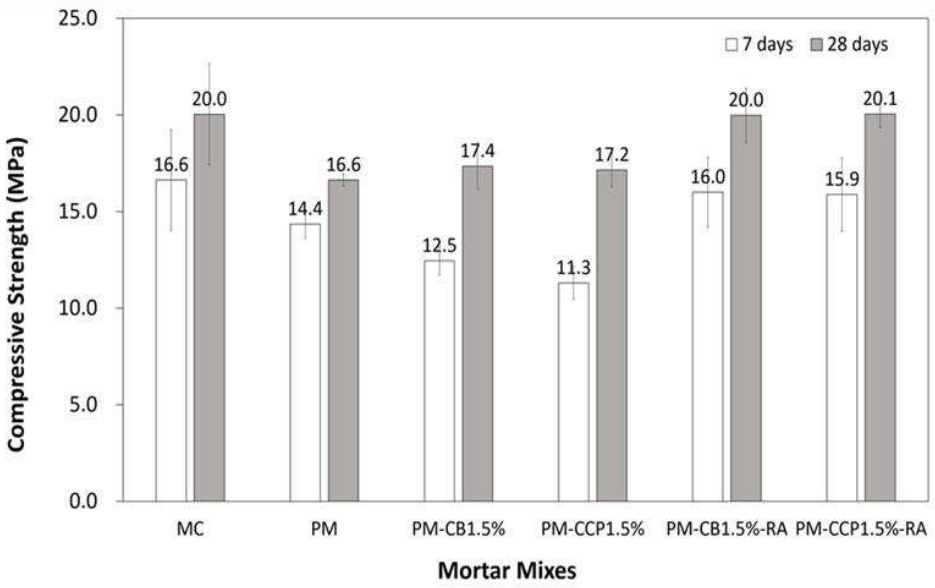


Figure 5. Compressive strength development of mortar mixtures incorporating pozzolan, bamboo/coco-peat cellulose fiber, and recycled brick aggregate at 7 and 28 days.

The use of recycled aggregate (RA) in fiber-modified pozzolan mortars was associated with a clear increase in compressive strength. The PM-CB1.5%-RA mixture attained 16.0 MPa at 7 days and 20.0 MPa at 28 days, whereas PM-CCP1.5%-RA achieved 15.9 MPa and 20.1 MPa, respectively. These values are similar or slightly higher than the normal mortar (MC). This enhancement can be explained by several factors that are consistent with mechanisms reported in the literature for recycled aggregate mortars: (1) an internal curing effect of the porous recycled aggregate, which holds and gradually releases water, allowing for continued cement hydration; (2) an improved interfacial transition zone (ITZ) due to the rough surface texture of recycled brick particles, which enhances mechanical interlocking between the aggregate and the mortar matrix (Chang et al., 2022; Islam et al., 2025); and (3) a synergistic interaction between the pozzolanic material, fibers, and recycled aggregate, resulting in a denser microstructure at later ages (Wang et al., 2025). The strength recovery observed here is also consistent with the reports that fine recycled clay-brick aggregate can densify the interfacial transition zone through its own latent pozzolanic activity and surface roughness when the replacement ratio and added water are adequately controlled (Dang et

al., 2018). Recent modeling of the interfacial transition zone (ITZ) of recycled aggregate concrete supports this idea. It indicates that the ITZ and its pore structure, not the recycled aggregate itself, are the main factors that affect compressive strength recovery. Denser, better bonded ITZs lead to disproportionately large gains in overall strength (Lu et al., 2024).

4.2.3 Flexural Strength

Figure 6 shows the 28-day flexural strength of the six mixtures. The control mortar (MC) reached 4.28 MPa. Replacing 60% of the cement with fly ash, limestone, and metakaolin increased the flexural strength of PM to 4.90 MPa, about 14% above MC, even though its 28-day compressive strength was lower (16.6 versus 20.0 MPa), so that the flexural-to-compressive strength ratio rose from about 0.21 to 0.30. This higher ratio is not fully explained by the present data; it may be related to the improved particle packing provided by the fine limestone and fly ash particles and to the pore refinement associated with metakaolin and the carboaluminate phases identified by XRD (Section 4.3.2; Zunino and Scrivener, 2020). The load–displacement curves (Figure 7) indicate that it is also related to the larger deformation capacity of the pozzolan matrix. PM-CB1.5% gave the highest flexural strength of all mixtures, 5.61 MPa, which is about 31% higher than MC and 14% higher than PM. This confirms the beneficial role of bamboo cellulose in flexure and is consistent with reports that alkali-treated bamboo and coir fibers act as crack-bridging elements that delay crack initiation and propagation and increase energy absorption during loading (Ahmad et al., 2022; Pederneiras et al., 2021). The gain is notable because the same fiber reduced the 7-day compressive strength of the pozzolan mortar, which indicates that bamboo cellulose contributes mainly through tensile stress transfer across developing microcracks rather than through matrix densification. The small fiber diameter of approximately 3.4 μm provides a large number of potential bridging sites within the cementitious matrix.

In contrast, PM-CCP1.5% reached 4.98 MPa, practically the same as PM (+2%), although 16% above MC. At this dosage, cocopeat cellulose therefore neither improved nor impaired the flexural strength of the pozzolan mortar. Although the cocopeat cellulose had a smaller nominal diameter (ca. 2.26 μm), a smaller size does not necessarily translate into higher reinforcing efficiency. The finer particles have a larger specific surface area and need more water and paste to be wetted and dispersed; most of the CCP agglomerated, and such agglomerates act as soft, porous inclusions

rather than as crack-bridging fibers. In addition, XRD indicated that CCP retarded early clinker hydration more strongly than CB (Section 4.3.2), and SEM showed no cocopeat fibers bridging pores (Section 4.3.1). These observations agree with recent work on untreated coconut fiber mortar, which showed that flexural gains are very sensitive to fiber length, dosage, and dispersion quality, and that poorly optimized combinations give little or no improvement over the unreinforced matrix (Alenezi et al., 2025). It should be noted that the CCP dosage was not optimized separately; the 1.5% dosage was selected from the bamboo series (Section 3.2), and a lower CCP content may perform better.

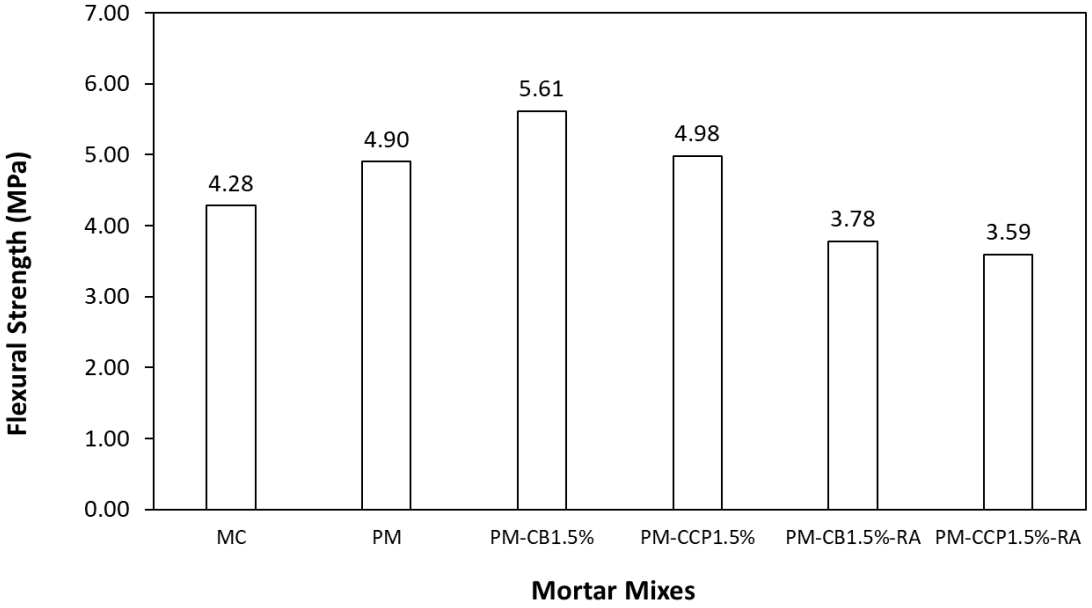


Figure 6. Flexural strength of different types of mortar at 28 days

Figure 7 shows the load–displacement curves of representative specimens of the six mixtures. The curves are stepped because the load was applied in increments and the displacement was read at intervals of about 0.01 mm; they therefore describe the pre-peak response well but cannot capture a post-peak softening branch, which would require displacement- or crack-opening-controlled loading. The peak loads, approximately 2,060 N (PM-CB1.5%), 1,980 N (PM-CCP1.5%), 1,760 N (PM), 1,400 N (MC), 1,350 N (PM-CB1.5%-RA), and 1,270 N (PM-CCP1.5%-RA), rank in the same order as the mean flexural strengths in Figure 6. MC was much stiffer than all the pozzolan mixtures: its load rose almost linearly, reaching about 600 N at 0.06 mm, when the pozzolan mixtures carried only about 170–260 N, and it failed at the smallest displacement, about 0.16 mm. The pozzolan mixtures followed a softer, upward-curving path, consistent with the lower elastic

modulus of a binder in which 60% of the cement was replaced and in which the pozzolanic reaction was still incomplete at 28 days (Section 4.3.2); part of the low initial slope may also reflect seating of the specimen on the rollers. However, they deformed further before failure (0.17–0.23 mm). The pozzolanic binder therefore exchanged stiffness for deformation capacity, which explains how PM reached a higher flexural strength than MC despite its lower compressive strength.

The bridging effect of bamboo cellulose is seen most clearly by comparing PM-CB1.5% with PM. Up to about 0.17 mm, the two curves are nearly superimposed, together with those of the two RA mixtures, which indicates that before cracking, the response is governed by the pozzolanic matrix and the fibers carry little load. Beyond this point the curves separate: PM failed at about 0.20 mm, whereas PM-CB1.5% continued to carry an increasing load up to about 0.23 mm and reached the highest peak load of all specimens. This extension of the ascending branch, in both load and displacement, is the signature of fibers transferring tensile stress across microcracks that form in the most highly stressed region of the beam, delaying their coalescence into a single critical crack. It is consistent with the SEM observation of intact, alkali-treated bamboo fibers spanning pores with both ends anchored in the matrix (Section 4.3.1). PM-CCP 1.5% behaved differently. It carried the lowest load of the pozzolan mixtures at every displacement; specifically, cocopeat cellulose made the matrix more compliant, which is consistent with its agglomerates acting as soft inclusions and its stronger retardation of early hydration. It nevertheless reached a displacement similar to that of PM-CB1.5% (about 0.23 mm) and a peak load about 12% above that of PM. Because SEM showed no cocopeat fibers bridging pores, this extended deformation is attributed mainly to the lower stiffness of the matrix rather than to crack bridging: cocopeat cellulose allowed more deformation at a lower load, whereas bamboo cellulose carried a higher load at the same deformation, which is why only bamboo cellulose produced a meaningful gain in flexural strength. None of the mixtures showed a post-peak softening branch; the curves of MC, PM, and the two fiber mixtures without RA end at their peak load. Within the limits of this load-controlled test, neither cellulose provided measurable post-cracking ductility at a dosage of 1.5%: once the critical crack opened beyond a few micrometers, the short micro-fibers could no longer bridge it. The benefit of bamboo cellulose therefore lies in delaying crack localization and increasing the peak load rather than in toughening the mortar. These results confirm that the effect of cellulose reinforcement depends on its compatibility with the pozzolanic matrix and not only on fiber size, as also reported for coir and cocopeat mortars (Alenezi et al., 2025; De Silva & Naveen, 2024).

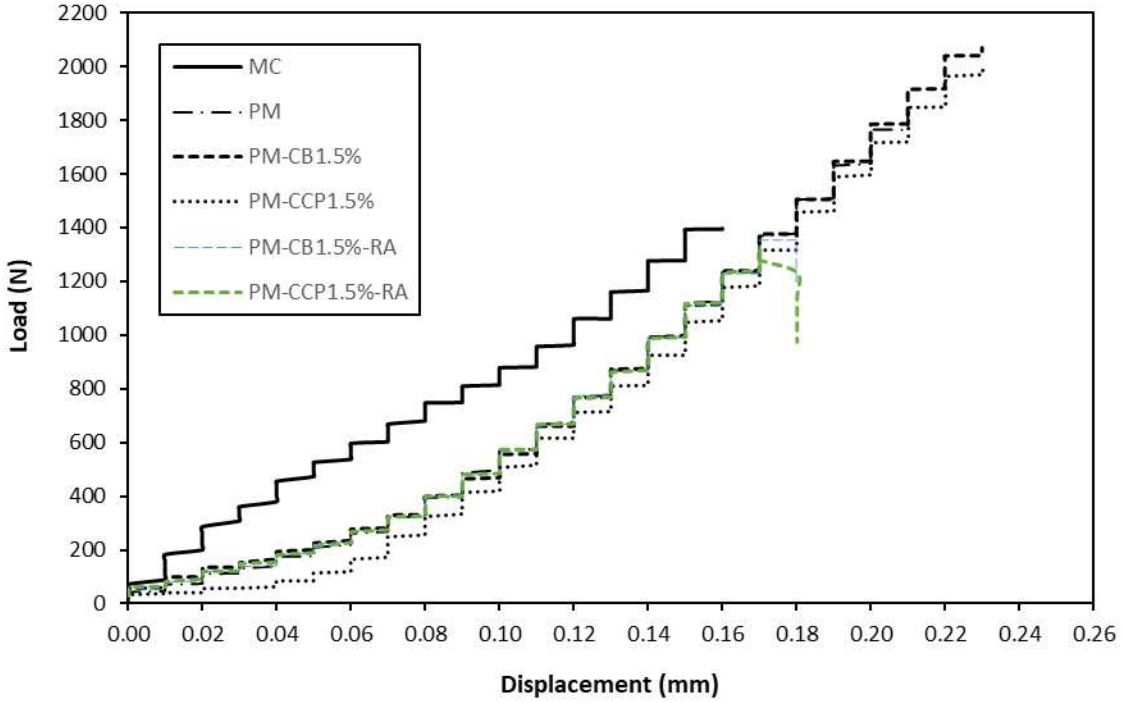


Figure 7. Load–displacement curves of mortar specimens at 28 days

Replacing 20% of the natural sand with recycled brick aggregate produced the largest flexural losses in this study. The flexural strength of the bamboo mixture fell from 5.61 MPa (PM-CB1.5%) to 3.78 MPa (PM-CB1.5%-RA), a reduction of about 33%, and that of the cocopeat mixture fell from 4.98 MPa (PM-CCP1.5%) to 3.59 MPa (PM-CCP1.5%-RA), a reduction of about 28%. Both RA mixtures were therefore about 23–27% below PM and 12–16% below MC, so RA cancelled the entire flexural benefit of both the pozzolanic binder and the celluloses. This contrasts with their compressive behavior: the RA mixtures reached the highest 28-day compressive strengths of the pozzolan mixtures (20.0–20.1 MPa), so their flexural-to-compressive strength ratio fell to about 0.18–0.19, the lowest of all mixtures. The load–displacement curves show how RA acted. Up to about 0.16 mm, both RA mixtures followed the PM curve, so RA did not reduce the stiffness before cracking; instead, they failed much earlier, at about 0.17–0.18 mm and 1,270–1,350 N. RA therefore lowered the load at which the critical crack formed rather than the slope of the curve. The interfacial transition zone around porous clay-brick particles is weaker than that around natural sand (Chang et al., 2022) and provides early crack initiation sites and straightforward paths along which flexural cracks can propagate and bypass the fibers. The porous brick particles also absorb

part of the mixing water, which may reduce the water available to wet and disperse the fibers and leave a more porous, less well-bonded paste around them, shortening the effective anchorage on which bridging depends. The larger loss in the bamboo mixture, together with the vertical load drop of PM-CB1.5%-RA at its peak, indicates that the crack-bridging contribution of bamboo cellulose was largely lost in the presence of RA. PM-CCP1.5%-RA was the only mixture with a short descending segment, from about 1,270 N to about 1,200 N, before the final drop to about 970 N; this behaviour may reflect a more tortuous crack path around brick particles and cellulose agglomerates, but because it rests on a single reading of one specimen under load control, it should not be interpreted as post-cracking toughness. The slightly higher strength of PM-CB1.5%-RA than of PM-CCP1.5%-RA (3.78 versus 3.59 MPa, about 5%), mirrored by its slightly higher peak load, suggests that a small part of the bamboo bridging survived. A similar compressive–flexural trade-off has been reported for masonry mortars combining recycled aggregate and natural fibers, in which recycled aggregate maintained or improved compressive strength while flexural strength was the more sensitive property (Ferrández et al., 2024). Because RA mixtures without cellulose were not tested and the RA mixtures were not examined by SEM, these mechanisms remain to be confirmed.

Overall, the effectiveness of cellulose reinforcement depends not only on fiber size or dosage but also on fiber morphology, dispersion, water demand, matrix composition, and aggregate–matrix interaction. Bamboo cellulose was clearly more effective than cocopeat cellulose in the pozzolan mortar: it raised both the peak load and the deformation at failure, whereas cocopeat cellulose at 1.5% mainly reduced the stiffness and left the flexural strength practically unchanged. The incorporation of recycled brick aggregate removed the advantages of both celluloses and lowered the flexural strength below that of the control mortar.

4.3 Microstructural Analysis

4.3.1 Scanning Electron Microscopy

Figures 8 and 9 show SE micrographs of paste samples after 28 days of curing together with the EDS spectrum of a representative spot in each sample, and Table 3 summarizes the corresponding compositions. As noted in Section 3.5, the EDS results are semi-quantitative; they are therefore interpreted together with the XRD results of the same mixtures (Section 4.3.2), which describe the

crystalline phase assemblage. The spot was selected as a representative of spectrums to evaluate the hydration mechanism after using the bamboo and cocopeat cellulose fibers in the mixtures.

Table 3. EDS composition (wt%) and atomic ratios at representative spots after 28 days

Mix	**Spot**	**Ca**	**Si**	**Al**	**Fe**	**Ca/Si (at.)**	**Al/Si (at.)**	**Interpretation**
MC	Spectrum 1	39.7	14.2	0.4	–	1.96	0.03	C-S-H intermixed with portlandite
PM	Spectrum 2	4.8	20.1	12.7	20.2	0.17	0.66	Partially reacted Fe-rich fly ash particle
PM-CB1.5%	Spectrum 4	6.3	20.8	17.5	–	0.21	0.88	Aluminosilicate grain (likely metakaolin)
PM-CCP1.5%	Spectrum 4	23.8	6.7	6.4	7.2	2.49	0.99	Ca-rich hydrates with Al-bearing (AFm) phases

Note: – = not detected. Atomic ratios were calculated from the measured wt% using standard atomic masses.

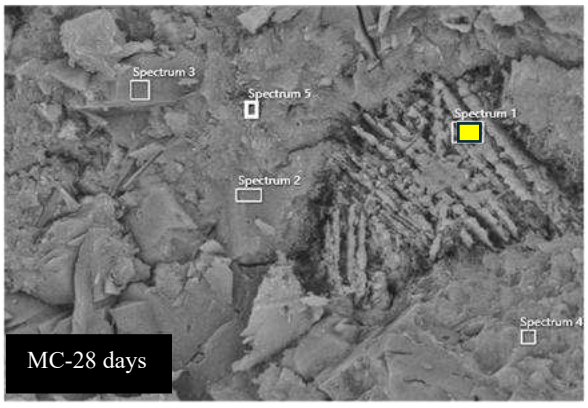
The control mortar (Figure 8a) shows a dense fracture surface in which stacks of lamellar, plate-like crystals, characteristic of portlandite, are embedded in a massive hydrate matrix. The spot on the lamellar region (Spectrum 1) contains mainly Ca and Si with almost no Al, giving an atomic Ca/Si ratio of 1.96. This value is above the range usually reported for C-S-H in Portland cement pastes (about 1.7–1.8), indicating that the analyzed volume contains C-S-H intermixed with portlandite (Scrivener et al., 2016). This agrees with the XRD results, in which portlandite was the strongest crystalline phase of MC at both ages.

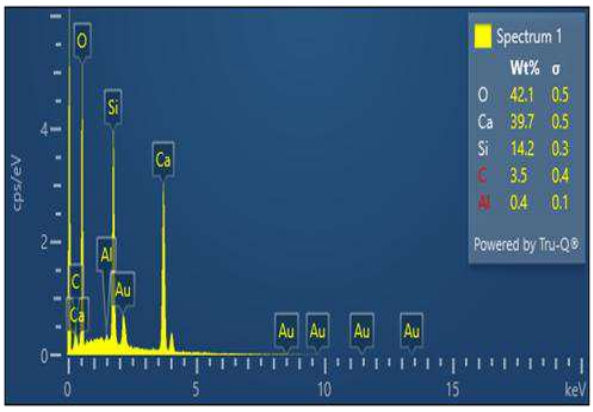
The micrograph of PM (Figure 8b) is dominated by a large, rounded particle with a pitted surface that is partly separated from the surrounding matrix by a thin gap. The spot on this particle (Spectrum 2) is rich in Si, Al, and Fe (20.2 wt%) and contains little Ca (atomic Ca/Si = 0.17). This composition matches the Fe-rich fly ash used in this study (Table 1) and the hematite and magnetite detected in it by XRD, so the particle is identified as a partially reacted fly ash grain rather than a hydration product. The pitted surface suggests that dissolution had begun, but the grain remained largely intact after 28 days. This is consistent with the XRD finding that portlandite was almost fully consumed while the pozzolanic reaction of the fly ash was still incomplete at 28 days, and it helps explain why the 28-day compressive strength of PM (16.6 MPa) remained below that of MC (20.0 MPa).

In PM-CB1.5% (Figure 9a), a bundle of straight, smooth bamboo cellulose fibers spans a pore with both ends embedded in the surrounding matrix, and clusters of fine-grained hydration

products line the pore walls. The fibers show no visible fragmentation or surface pitting, which suggests that the alkali-treated bamboo cellulose had not been noticeably degraded in the alkaline pore solution after 28 days. Fibers that cross a void while remaining anchored on both sides are in the configuration required to bridge a crack, which is consistent with the highest flexural strength (5.61 MPa) and the more extended load–displacement response of this mixture (Section 4.2.3). The matrix spot (Spectrum 4) contains mainly Si and Al with little Ca (atomic Ca/Si = 0.21, Al/Si = 0.88) and minor K and Ti; this is the composition of an aluminosilicate grain, most likely partially reacted metakaolin, rather than of a hydration product. Because the fibers lie within a pore over much of their visible length, this image alone cannot establish the quality of the fiber–matrix bond; higher-magnification imaging of fiber pull-out sites would be needed to assess it.

The fracture surface of PM-CCP1.5% (Figure 9b) is compact and fine-grained, with plate-like and fragmented hydrates. Only one thin, elongated cocopeat fiber can be identified (arrow), lying flat within the fracture plane and largely covered by hydration products; elsewhere individual fibers are difficult to distinguish, which is consistent with the fine and largely agglomerated morphology of this cellulose (Section 2). The analyzed spot (Spectrum 4) is Ca-rich (atomic Ca/Si = 2.49) and also contains appreciable Al (Al/Si = 0.99), Fe, and C. A Ca/Si ratio this high, combined with high Al and C contents, indicates that the analyzed volume is dominated by portlandite and/or calcite intermixed with Al-bearing phases rather than by C-S-H alone. This is in line with the XRD results, which showed that PM-CCP1.5% contained the largest amount of carboaluminate AFm phases of all mixtures at 28 days. Unlike the bamboo cellulose, no cocopeat fibers spanning pores or cracks were observed in the examined area, which agrees with the absence of a flexural gain in this mixture (4.98 MPa, compared with 4.90 MPa for PM and 5.61 MPa for PM-CB1.5%).





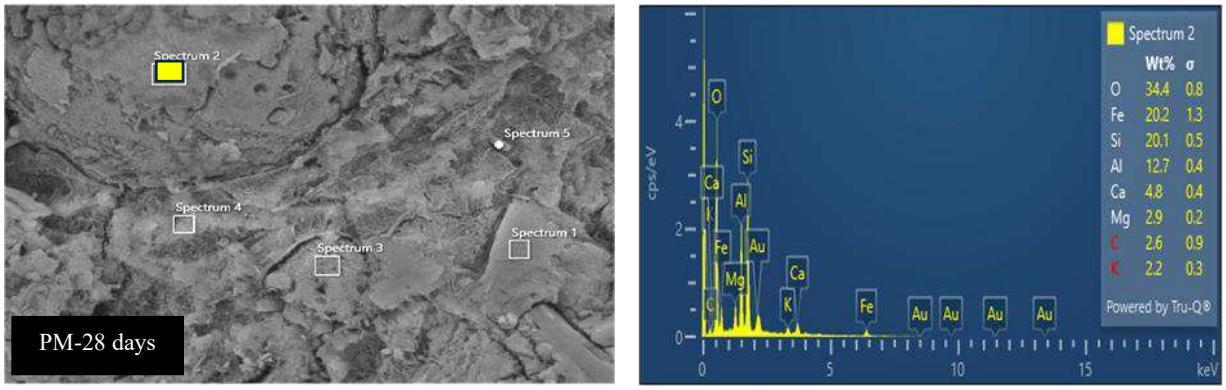


Figure 8. SEM micrographs (SE mode) and EDS spectra of representative spots in (a) MC, top row (Spectrum 1), and (b) PM, bottom row (Spectrum 2), at 28 days

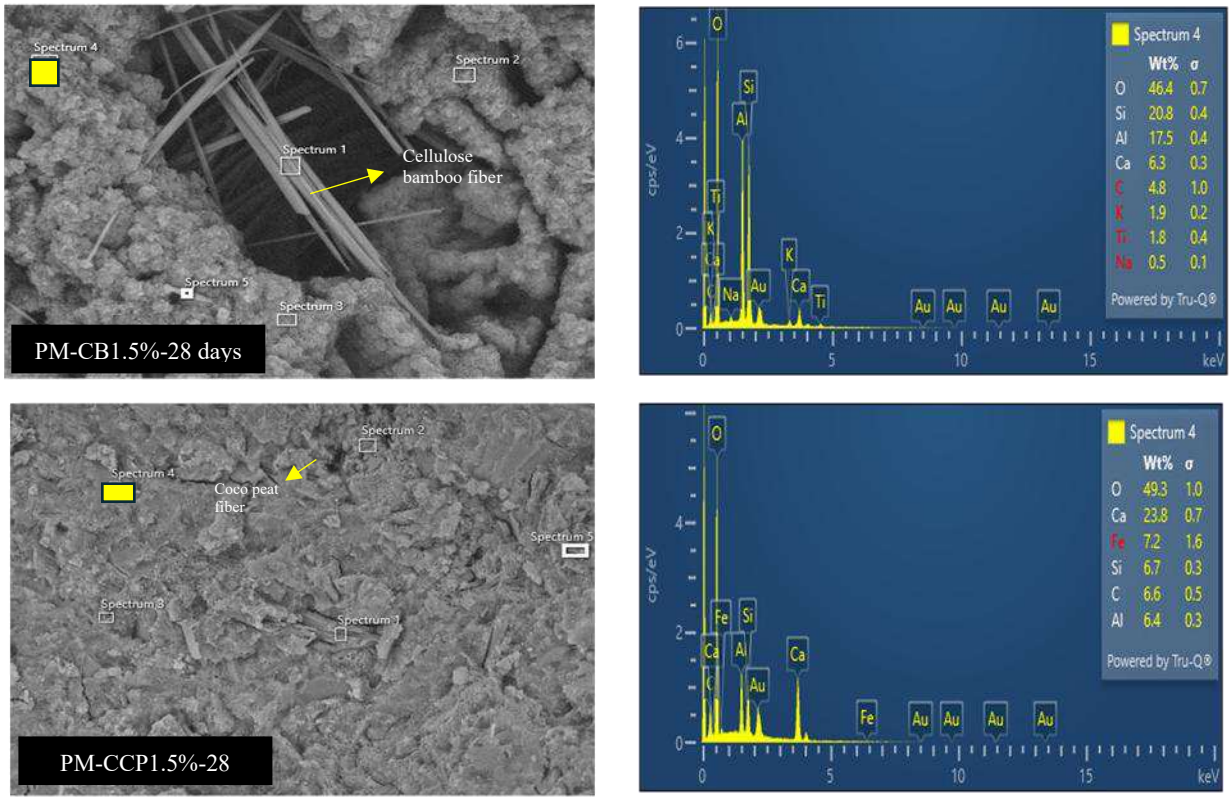


Figure 9. SEM micrographs (SE mode) and EDS spectra of representative spots in (a) PM-CB1.5%, top row, and (b) PM-CCP1.5%, bottom row (Spectrum 4), at 28 days

Taken together, the SEM-EDS observations qualitatively support the XRD and mechanical results: partially reacted fly ash persisted in PM at 28 days, bamboo cellulose fibers remained intact and were able to bridge pores, and cocopeat cellulose appeared only as isolated fibers lying within the matrix, without the pore-bridging configuration observed for bamboo cellulose. The mixtures

containing recycled brick aggregate were not examined by SEM, so the effects of RA on the interfacial transition zone discussed in Sections 4.2.2 and 4.2.3 are inferred from the mechanical results and from previous studies on clay-brick aggregates (Chang et al., 2022; Dang et al., 2018) rather than observed directly. Backscattered-electron imaging of polished sections with a larger number of EDS points, extended to the RA mixtures, would be required to quantify the C-S-H composition and the aggregate–paste interfaces (Scrivener et al., 2016; Zhang et al., 2025).

4.3.2 X-Ray Diffraction

The XRD patterns of the four mixes at 7 and 28 days are presented in Figure 10. All patterns contain the same principal crystalline phases: portlandite ($Ca(OH)_2$; $2\theta = 18.0°$, 28.7°, 34.1°, 47.1°, and 50.8°), calcite ($CaCO_3$; 23.0°, 29.4°, 36.0°, 39.4°, 43.2°, 47.5°, 48.5°, and 57.4°), ettringite (15.8° and 22.9°), the carbonate-bearing AFm phases monocarbonate (11.65°) and hemicarbonate (10.8°), and weak reflections of unhydrated alite/belite near 32.2°. C–S–H, the main binding phase, is nanocrystalline and does not produce sharp reflections; it appears as the broad diffuse hump between approximately 25° and 35° 2θ, on which the calcite reflection is superimposed. In the pozzolanic mixes, this hump also contains the contribution of the fly ash glass. The fly ash additionally introduces quartz (20.8° and 26.6°), hematite (33.2° and 35.6°), and magnetite (30.2° and 35.4°), which behaved as inert phases and remained essentially unchanged between 7 and 28 days. Because no internal standard was used, phase changes were evaluated semi-quantitatively from the background-subtracted integrated intensities of the diagnostic reflections. This approach is suitable for comparing trends between samples measured under identical conditions, but not for absolute phase quantification (Scrivener et al., 2016).

The control mortar (MC) is dominated by portlandite, whose reflection at 18.0° is the strongest peak of the pattern (~23,000 counts at 7 days). Its intensity decreased by about 30% between 7 and 28 days, whereas the reflection at 34.1° remained practically constant. The basal reflection of the platy portlandite crystals is strongly affected by preferred orientation during sample preparation (Scrivener et al., 2016); the portlandite content of MC is therefore better described as stable between the two ages. Together with the weak and unchanged clinker reflections, these observations indicate that most of the alite hydration in MC had already taken place by 7 days and that the further 20% gain in strength up to 28 days arises mainly from continued densification by C–S–H, which cannot be resolved by XRD. The intense calcite and monocarbonate reflections of

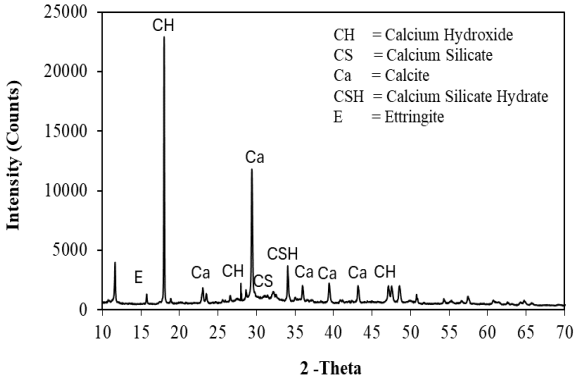
MC show that the reference cement itself contains limestone. In the presence of calcite, monocarbonate rather than monosulfate is the stable AFm phase, which indirectly stabilizes ettringite, increases the volume of hydrates, and reduces porosity (Lothenbach et al., 2008).

Replacing 60% of the cement with fly ash, limestone, and metakaolin changed the phase assemblage considerably. At 7 days, the portlandite intensity of PM was approximately 80% lower than that of MC, reflecting both the dilution of the clinker and the early consumption of portlandite by the highly reactive metakaolin. Between 7 and 28 days, the portlandite reflections of PM decreased by a further ~82%, almost to the detection limit, which is clear evidence of the pozzolanic reaction of fly ash and metakaolin. This agrees with Deschner et al. (2012), who showed that fly ash acts mainly as a filler at early ages and that its pozzolanic reaction becomes evident from about 7 days through the consumption of portlandite. Over the same period, the AFm reflections at 10.8–11.2° increased by about 25% and ettringite by about 20%, while calcite remained constant. The growth of carboaluminate AFm and the stabilization of ettringite are characteristic of the reaction between the alumina supplied by metakaolin and fly ash and the carbonate supplied by limestone (Antoni et al., 2012; Zunino and Scrivener, 2020). The unchanged calcite intensity indicates that only a small fraction of the limestone was consumed, so it acted predominantly as a filler and as the carbonate source for these AFm phases.

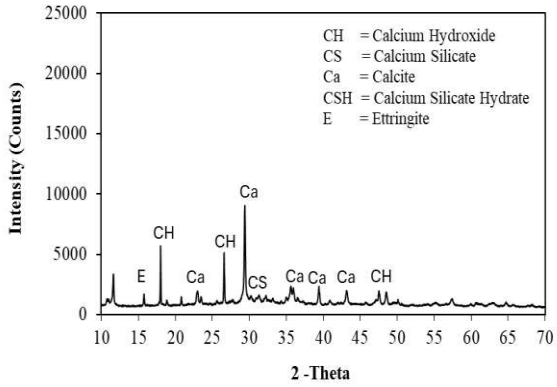
The addition of 1.5% bamboo cellulose (PM-CB1.5%) or cocopeat cellulose (PM-CCP1.5%) did not generate new crystalline phases at 7 days but modified the relative amounts of the existing hydrates, in agreement with Agunbiade and Mangat (2025), who found that nanocellulose alters the crystallinity of the hydration products rather than their type. The portlandite (001) intensity of PM-CB1.5% and PM-CCP1.5% was about 66% and 73% lower than that of PM, while the residual clinker reflections were comparable. Because the 7-day strength of these mixes was also lower than that of PM, the reduced portlandite cannot be attributed to an accelerated pozzolanic reaction; it indicates instead that the hydration of alite was retarded. Lignocellulosic materials release sugars, hemicellulose degradation products, and other extractives into the alkaline pore solution, which adsorb on the cement grains and delay the hydration of C_3S (Govin et al., 2006; Bołtryk et al., 2025). In addition, $Ca(OH)_2$ can migrate into and precipitate within the lumen, walls, and voids of natural fibers (Tolêdo Filho et al., 2000), where it is poorly crystalline and contributes little to either the diffraction signal or the strength. The stronger effect of cocopeat is consistent with its higher content of fine, extractive-rich pith particles. In contrast, the AFm reflections of PM-

CCP1.5% were already about 74% higher than those of PM at 7 days, indicating that the aluminate reactions of metakaolin and limestone were less affected by the cellulose than the silicate hydration.

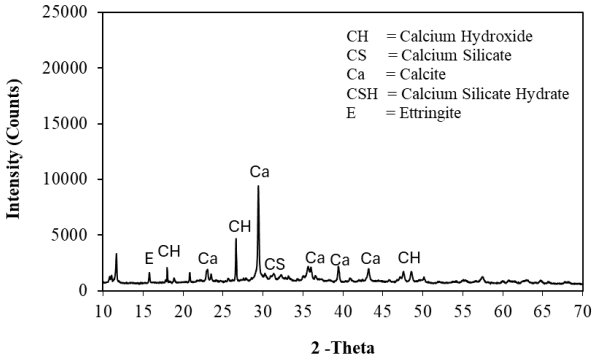
Between 7 and 28 days, the cellulose-modified mixes evolved differently from PM. In PM-CB1.5%, the portlandite intensity did not decrease (+9%), whereas the AFm reflections increased by about 76%, reaching a level 44% higher than that of PM at 28 days. The stable portlandite level suggests that the delayed hydration of the clinker continued to produce portlandite at a rate similar to its consumption by the pozzolans. In PM-CCP1.5%, portlandite decreased by about 36% and monocarbonate by about 13%, while a sharp reflection appeared at 10.92° (d = 8.10 Å) together with its second-order reflection at 21.98° (d = 4.04 Å). This pair of basal reflections identifies a well-crystallized 8.1 Å AFm phase of the hemicarbonate/C_4AH_{13} type. It cannot be attributed to crystalline cellulose, which produces broad reflections near 22.5° and would already have been present at 7 days. Consequently, PM-CCP1.5% contained the largest amount of AFm of all mixes at 28 days (about 69% more than PM). The shift from monocarbonate towards the carbonate-poorer hemicarbonate points to a local excess of alumina relative to the available carbonate, as expected when metakaolin continues to react (Zunino and Scrivener, 2020). The continued hydration of the cellulose-modified mixes is consistent with the water-retention capacity of cellulose, which acts as an internal curing reservoir and facilitates the transport of water to unhydrated cement grains (Cao et al., 2015; Agunbiade and Mangat, 2025).



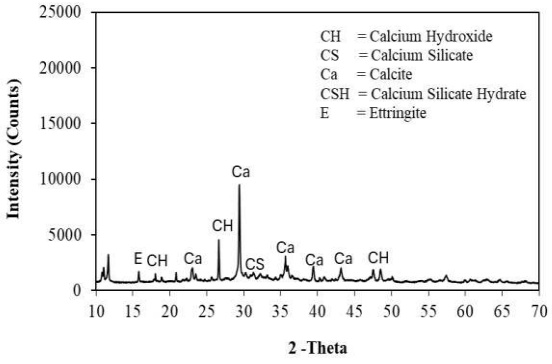
(a) MC – 7 days



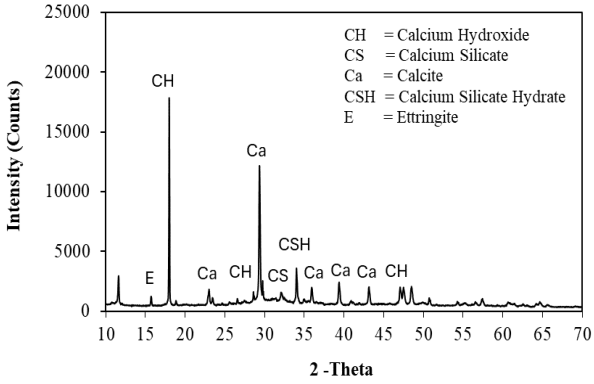
(b) PM – 7 days



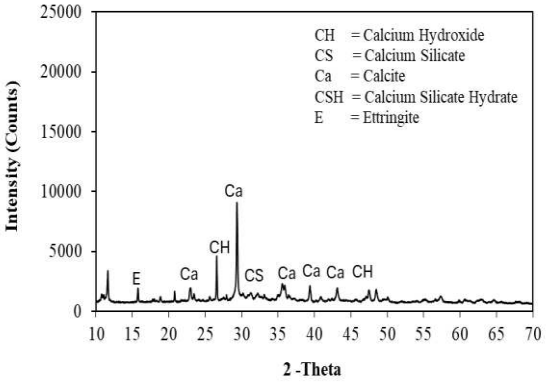
(c) PM-CB1.5% – 7 days



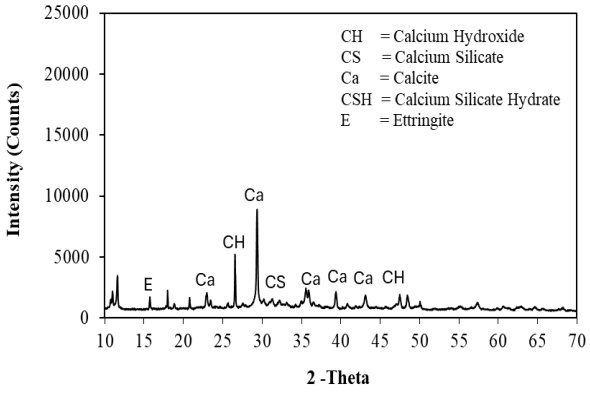
(d) PM-CCP1.5% – 7 days



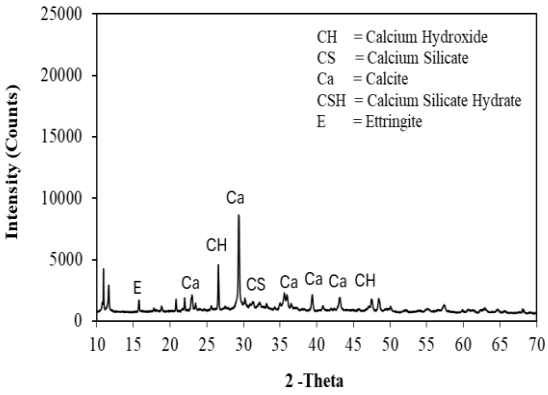
(e) MC – 28 days



(f) PM – 28 days



(g) PM-CB1.5% – 28 days



(h) PM-CCP1.5% – 28 days

Figure 10. XRD patterns of (a) MC, (b) PM, (c) PM-CB1.5%, and (d) PM-CCP1.5% at 7 days, and (e)–(h) the same mixes at 28 days (Cu Kα). CH = portlandite, Ca = calcite, E = ettringite, CS

= residual calcium silicates (C_3S/C_2S); the broad hump between ~25° and 35° 2θ corresponds to C–S–H (and fly ash glass in the PM mixes).

The XRD and compressive strength results are consistent. At 7 days, strength followed the amount of crystalline portlandite (MC > PM > PM-CB1.5% > PM-CCP1.5%; 16.6, 14.4, 12.5, and 11.3 MPa), confirming that early strength is controlled by the degree of clinker hydration and that the strength loss caused by the cellulose results from retarded alite hydration rather than from a change in the type of hydrates formed. Between 7 and 28 days, the largest strength gains were recorded for the mixes with the largest increase in AFm phases (+52% for PM-CCP1.5% and +39% for PM-CB1.5%, compared with +15% for PM). This indicates that continued hydration and the precipitation of carboaluminate phases, which refine the pore structure (Antoni et al., 2012; Zunino and Scrivener, 2020), compensated for the early delay so that both cellulose-modified mixes reached 28-day strengths comparable to that of PM (17.4 and 17.2 MPa versus 16.6 MPa). The almost complete consumption of portlandite in PM produced only a modest strength gain, showing that the pozzolanic reaction of the fly ash was still incomplete at 28 days and that further strength development can be expected at later ages (Deschner et al., 2012). MC retained the highest strength (20.0 MPa) owing to its higher clinker content and larger volume of C–S–H, even though its crystalline phase assemblage changed little between 7 and 28 days. Overall, the phase analysis shows that 1.5% bamboo or cocopeat cellulose delays the early hydration of the fly ash–limestone–metakaolin binder but promotes later hydration and AFm formation so that the 28-day compressive strength is comparable to, or slightly higher than, that of PM.

4.4 Environmental Assessment

The CO_2 emissions of the mixtures were estimated from the material quantities in Table 2 and cradle-to-gate emission factors, following the calculation of Total CO_2 per m^3 = Σ (material mass per m^3 × emission factor), whereas transport and mixing energy were excluded. The emission factors of PCC, fly ash, limestone, and natural sand were 0.668, 0.006, 0.0245, and 0.011 kg CO_2/kg, respectively. Metakaolin was taken as 0.20 kg CO_2/kg, and the recycled brick aggregate as 0.006 kg CO_2/kg, which accounts only for crushing, since the waste brick carries no production burden. For the treated cellulose, a factor of 1.0 kg CO_2/kg was estimated from the NaOH consumption of the treatment (0.8 kg NaOH per kg of cellulose at an assumed yield of 50%). This

factor excludes the energy used for heating during alkali treatment (3 h at 80–100 °C) and for oven drying (24 h at 60 °C), so it should be regarded as a lower bound.

Table 4. Estimated cradle-to-gate CO_2 emissions per m^3 of low-carbon mortar containing cellulose fiber and recycled aggregate

Material	**Emission factor (kg CO_2/kg)**	**Total emission (t CO_2/m^3)**					
		Normal	PM	PM-CB1.5%	PM-CCP1.5%	PM-CB1.5%-RA	PM-CCP1.5%-RA
Cement	0.668	0.3340	0.1336	0.1336	0.1336	0.1336	0.1336
Metakaolin	0.2	0.0000	0.0050	0.0050	0.0050	0.0050	0.0050
Limestone	0.0245	0.0000	0.0018	0.0018	0.0018	0.0018	0.0018
Fly ash	0.006	0.0000	0.0012	0.0012	0.0012	0.0012	0.0012
Fine Aggregate	0.011	0.0110	0.0110	0.0110	0.0110	0.0088	0.0088
Recycled Aggre-gate	0.006	0.0000	0.0000	0.0000	0.0000	0.0012	0.0012
Treated cellulose	1	0.0000	0.0000	0.0075	0.0075	0.0075	0.0075
Total		0.345	0.153	0.160	0.160	0.159	0.159

The cradle-to-gate CO_2 emissions of the mixtures were calculated from the quantities in Table 2 and the emission factors in Table 4. The factors come from the Inventory of Carbon and Energy (ICE) database (Circular Ecology), except for the treated cellulose. No ICE value exists for alkali-treated cellulose, so its factor (1.0 kg CO_2/kg) was estimated from the NaOH consumed during the treatment. Transport, mixing, and the superplasticizer were excluded. The carbon assessment shows that cement dominated the footprint of the normal mix, accounting for about 96.8% of its total emission (0.334 of 0.345 t-CO_2). Partially replacing cement with fly ash, limestone, and metakaolin in the PM mix lowered the total emission to 0.153 t-CO_2, a 55.7% reduction compared with the normal mix. Adding 1.5% treated cellulose (PM-CB1.5% and PM-CCP1.5%) slightly raised the emission to 0.160 t-CO_2, about 4.9% higher than PM, because of the energy-intensive fiber treatment. Even so, these mixes remained 53.6% lower in carbon than the normal mix. Because the cellulose raised the 28-day compressive strength by a similar proportion (17.4 and 17.2 MPa versus 16.6 MPa), the emission per unit of compressive strength remained practically unchanged: about 0.0092–0.0093 t CO_2/m^3 per MPa for PM, PM-CB1.5%, and PM-CCP1.5%, compared with 0.0173 for MC and 0.0079–0.0080 for the two RA mixtures. Replacing 20% of the natural sand with recycled brick aggregate (PM-CB1.5%-RA and PM-CCP1.5%-RA) further

reduced the emission to 0.159 t-CO_2, a 53.9% reduction relative to the normal mix. The direct carbon saving from the recycled aggregate is modest, but its sustainability value goes beyond the emission figure: it diverts construction and demolition waste from landfill and conserves natural sand resources. Overall, combining pozzolanic binders, bio-based cellulose fiber from agricultural and bamboo resources, and recycled brick aggregate produces a mortar with less than half the carbon footprint of conventional mortar, while also promoting waste valorization and a circular use of materials.

4.5 Potential Development of Low-Carbon Mortar with bio-based cellulose reinforcement for Sustainable Construction

The developed mortar demonstrates a multi-dimensional approach to sustainable construction through the simultaneous reduction of Portland cement, utilization of industrial and agricultural by-products, incorporation of recycled construction waste, and application of bio-based cellulose reinforcement. The binder consists of 40% PCC, 40% fly ash, 15% limestone, and 5% metakaolin, resulting in a total PCC replacement level of 60%. This substantial reduction in PCC has significant potential to decrease the clinker-related embodied carbon of the mortar, while the incorporation of fly ash promotes the beneficial utilization of an industrial by-product. Limestone provides an additional low-clinker constituent and can contribute to particle packing and carbonate-related reactions, whereas metakaolin provides a highly reactive aluminosilicate component that can enhance the development and refinement of the cementitious matrix. The 20% replacement of natural sand with recycled brick aggregate further extends the sustainability benefits by diverting construction and demolition waste from disposal and reducing demand for virgin aggregate resources. Recycled aggregate systems, however, commonly exhibit increased water absorption and porosity, which can adversely affect mechanical performance and therefore require appropriate mixture optimization. This finding is consistent with recent work on brick-waste valorization in circular construction materials, which similarly reports that untreated brick-derived constituents require careful mixture-level optimization to balance their pozzolanic and water-absorptive characteristics against mechanical performance targets (Mildner et al., 2025).

The incorporation of bio-based cellulose provides an additional pathway for improving the sustainability and functional performance of the mortar. Bamboo cellulose at 1.5% of binder mass increased the measured flexural strength from 4.90 to 5.61 MPa and produced a more extended

load–displacement response, indicating enhanced crack-bridging and stress-transfer capacity. On the other hand, cocopeat cellulose at the same dosage left the flexural strength practically unchanged (4.98 MPa), although its utilization remains environmentally relevant as a pathway for valorizing agricultural biomass. The loss of the cellulose benefit and the drop in flexural strength below that of the control mortar when 20% recycled brick aggregate was incorporated indicate an interaction between fiber reinforcement and the recycled aggregate–matrix interfacial characteristics. Thus, the sustainability of the proposed mortar should be understood as a performance-based balance between clinker reduction, waste valorization, natural-resource conservation, renewable reinforcement, and mechanical performance rather than as a simple maximization of waste content. Recent research similarly emphasizes that low-carbon construction materials require simultaneous consideration of embodied carbon, strength, durability, processing, and material availability (Mildner et al., 2025; Zhang et al., 2025).

5. Conclusions

Based on the results, some conclusions can be drawn as follows:

1. Bamboo cellulose fiber improved the compressive strength of plain cement mortar, achieving an optimum dosage of 1.5% of the total binder. The 28-day compressive strength increased from 25.3 MPa for the control to 29.9 MPa for the 1.5% dosage, but the strength was reduced below the control value at the 2% dosage.
2. The partial replacement of Portland cement with 40% fly ash, 15% limestone, and 5% metakaolin, together with the addition of cellulose fiber, led to a reduction of early-age (7-day) compressive strength of up to 32% compared to the control mortar. At 28 days, the fiber mixtures (17.2–17.4 MPa) slightly exceeded the plain pozzolan mortar (16.6 MPa) but remained 13–14% below the control (20.0 MPa). The mixtures containing recycled brick aggregate, PM-CB1.5%-RA and PM-CCP1.5%-RA, reached 28-day compressive strengths of 20.0 and 20.1 MPa, respectively, equal to that of the control.
3. The flexural strength followed a different trend from the compressive strength. The pozzolanic binder increased the flexural strength from 4.28 MPa (MC) to 4.90 MPa, and bamboo cellulose increased it further to 5.61 MPa (about 31% above MC and 14% above PM). The load–displacement curves showed that bamboo cellulose raised both the peak load and the displacement at failure of the pozzolan mortar, consistent with microcrack

bridging, although no mixture showed post-peak softening. Cocopeat cellulose made the pozzolan mortar more compliant and left its flexural strength practically unchanged (4.98 MPa). Recycled brick aggregate reduced the flexural strength of the bamboo and cocopeat mixtures by about 33% and 28% (to 3.78 and 3.59 MPa), below that of the control mortar, by lowering the load at which the critical crack formed, indicating that RA weakens the crack-bridging contribution of the fibers.

4. SEM-EDS at 28 days showed intact bamboo cellulose fibers bridging pores in PM-CB1.5%, consistent with its higher flexural strength, and partially reacted Fe-rich fly ash particles in PM, consistent with the incomplete pozzolanic reaction indicated by XRD. Cocopeat cellulose appeared only as isolated fibers embedded in the matrix, without pore bridging, in line with the absence of a flexural gain over PM.
5. XRD showed that all mixes contained portlandite, calcite, ettringite, and carboaluminate AFm phases, with C-S-H present as an amorphous hump. Replacing 60% of the cement with fly ash, limestone, and metakaolin (PM) consumed almost all the portlandite by 28 days through the pozzolanic reaction and increased the carboaluminate and ettringite content. Adding 1.5% bamboo or cocopeat cellulose formed no new phases, but it retarded early clinker hydration, giving lower portlandite and lower strength at 7 days. Between 7 and 28 days, the cellulose mixes formed much more AFm, most of all PM-CCP1.5%, and this matched their larger strength gains and 28-day strengths comparable to PM.
6. Recycled brick aggregate offset the compressive-strength penalty of pozzolan substitution and cellulose fiber addition so that PM-CB1.5%-RA and PM-CCP1.5%-RA reached the compressive strength of the control mortar, albeit with a lower flexural strength, while at the same time reducing clinker content, valuing agricultural waste and construction/demolition waste, and incorporating renewable fiber reinforcement. Future work should prioritize (i) confirming the proposed hydration and ITZ mechanisms against SEM/EDS micrographs through quantitative image analysis; (ii) hybrid fiber reinforcement, for example, combining bamboo and coco peat cellulose or supplementing bamboo cellulose with mineral micro-reinforcement to recover the flexural strength lost upon recycled-aggregate incorporation, following the orthogonal optimization approach recently used to balance natural-fiber content, fiber length, and water-cement ratio in bamboo-fiber recycled-aggregate concrete (Xu et al., 2024); (iii) pre-treatment of the

recycled brick aggregate, such as surface coating or controlled pre-wetting, to densify its interfacial transition zone; and (iv) durability and life-cycle assessment of the PM-CB1.5%-RA and PM-CCP1.5%-RA mixtures to quantify their embodied-carbon and waste-valorization benefits relative to conventional mortar. The work overall indicates the technical feasibility of combining bio-based fibers and waste-derived constituents for low-carbon, circular mortar production, with flexural performance identified as the key constraint requiring further optimization.

7. From an environmental perspective, partially replacing cement with fly ash, limestone, and metakaolin reduced CO_2 emissions by 55.7% compared with conventional mortar. Adding 1.5% cellulose increased emissions only slightly, and the mixes still achieved a reduction of about 53.6%. Replacing 20% of the sand with recycled brick aggregate lowered emissions further, to 53.9% below the conventional mix, while also reusing construction waste and conserving natural sand. Overall, combining pozzolanic binders, cellulose fiber, and recycled brick aggregate is a promising route to mortar with less than half the carbon footprint of conventional mortar and a compressive strength equal to that of conventional mortar, although flexural strength remains the main limitation of the mixtures containing recycled brick aggregate.

6. Acknowledgment

The authors would like to thank the National Research and Innovation Agency of the Republic of Indonesia (BRIN) for funding this research through the Research and Innovation for Advanced Indonesia (RIIM) program under Contract Number 95/IV/KS/04/2026.

Statements and Declarations

Funding

This research was funded by the National Research and Innovation Agency of the Republic of Indonesia (Badan Riset dan Inovasi Nasional, BRIN) through the Research and Innovation for Advanced Indonesia (RIIM) program under Contract Number 95/IV/KS/04/2026. The funder had no role in the study design, data collection, analysis and interpretation, writing of the manuscript, or the decision to submit it for publication.

Competing Interests

The authors have no relevant financial or non-financial interests to disclose.

Author Contributions

All authors contributed to the study conception and design. Steve W.M Supit: Conceptualization, Methodology, Supervision, Funding acquisition, Microstructure analysis, Writing original draft. Henry Aritonang: Investigation (cellulose extraction and fiber treatment), Priyono: Investigation (mortar preparation and mechanical testing), Debby Willar and Stefani Peginusa: Low carbon potential and sustainable construction. All authors read and approved the final manuscript.

Data Availability

The datasets generated and analyzed during the current study are available from the corresponding author on reasonable request.

Ethics Approval

Not applicable. This study did not involve human participants or animals.

Consent to Participate

Not applicable.

Consent for Publication

Not applicable.

References

Ahmad, J., Majdi, A., Al-Fakih, A., Deifalla, A. F., Althoey, F., El Ouni, M. H., & El-Shorbagy, M. A. (2022). Mechanical and durability performance of coconut fiber reinforced concrete: A state-of-the-art review. Materials, 15(10), 3601. https://doi.org/10.3390/ma15103601

Agunbiade, T., Mangat, P.S., 2025. Hydration products and properties of nanocellulose fiber-reinforced mortar. Sustainability 17(6), 2719. https://doi.org/10.3390/su17062719

Alenezi, D., Mohammad, D., Alfoudari, F., Saeedi, M., Alajmi, R., & Mustafaraj, E. (2025). Strength and water absorption behavior of untreated coconut fiber-reinforced mortars: Experimental evaluation and mix optimization. Construction Materials, 5(3), Article 69. https://doi.org/10.3390/constrmater5030069

Allujami, H. M., Abdulkareem, M., Jassam, T. M., Al-Mansob, R. A., Ng, J. L., & Ibrahim, A. (2022). Nanomaterials in recycled aggregate concrete applications: Mechanical properties and durability—A review. Cogent Engineering, 9(1), 2122885. https://doi.org/10.1080/23311916.2022.2122885

Antoni, M., Rossen, J., Martirena, F., Scrivener, K., 2012. Cement substitution by a combination of metakaolin and limestone. Cement and Concrete Research 42(12), 1579–1589. https://doi.org/10.1016/j.cemconres.2012.09.006

Bołtryk, M., Pawluczuk, E., Kalinowska-Wichrowska, K., et al., 2025. The influence of two-stage mineralization of organic fillers on the properties of cement composites. Archives of Civil and Mechanical Engineering 25(3), 127. https://doi.org/10.1007/s43452-025-01170-1

Cao, Y., Zavattieri, P., Youngblood, J., Moon, R., Weiss, J., 2015. The influence of cellulose nanocrystal additions on the performance of cement paste. Cement and Concrete Composites 56, 73–83.

Chang, J., Luo, S.-L., Ailifeila, A., Chong, L.-L., & Jiang, J.-Q. (2022). Effects of coarse and fine crushed clay brick content on the compressive strength of recycled aggregate concrete and the microscopic mechanism. Geofluids, 2022, Article 1341185. https://doi.org/10.1155/2022/1341185

De Silva, G. H. M. J. S., & Naveen, P. (2024). Effect of rice husk ash and coconut coir fiber on cement mortar: Enhancing sustainability and efficiency in buildings. Construction and Building Materials, 440, Article 137326. https://doi.org/10.1016/j.conbuildmat.2024.137326

Deschner, F., Winnefeld, F., Lothenbach, B., Seufert, S., Schwesig, P., Dittrich, S., Götz-Neunhoeffer, F., Neubauer, J., 2012. Hydration of Portland cement with high replacement by siliceous fly ash. Cement and Concrete Research 42(10), 1389–1400. https://doi.org/10.1016/j.cemconres.2012.06.009

Dang, J., Zhao, J., Hu, W., Du, Z., & Gao, D. (2018). Properties of mortar with waste clay bricks as fine aggregate. Construction and Building Materials, 166, 898–907. https://doi.org/10.1016/j.conbuildmat.2018.01.109

Ferrández, D., Zaragoza-Benzal, A., Pastor Lamberto, R., Santos, P., & Michalak, J. (2024). Optimizing masonry mortar: Experimental insights into physico-mechanical properties using recycled aggregates and natural fibers. Applied Sciences, 14(14), 6226. https://doi.org/10.3390/app14146226

Fu, X., Liu, P., Kong, D., Li, Y., & Wang, Y. (2025). Mechanical properties of raw bamboo fiber-reinforced phosphogypsum-based composite cementitious materials and their strengthening mechanism. PLOS ONE, 20(5), Article e0323011. https://doi.org/10.1371/journal.pone.0323011

Govin, A., Peschard, A., Guyonnet, R., 2006. Modification of cement hydration at early ages by natural and heated wood. Cement and Concrete Composites 28(1), 12–20.

Islam, Z. U., Farooq, S., Shoaib, M., Ishfaq, M., & Ahmad, T. (2025). Evaluating the mechanical properties of recycled aggregate concrete with variable aggregate replacements. Discover Civil Engineering, 2, 174. https://doi.org/10.1007/s44290-025-00336-3

Lu, C., Yu, Q., Wei, J., Niu, Y., Zhang, Y., Lin, C., Chen, P., Shi, C., & Yang, P. (2024). Influence of interface transition zones (ITZ) and pore structure on the compressive strength of recycled aggregate concrete. Construction and Building Materials, 456, Article 139299. https://doi.org/10.1016/j.conbuildmat.2024.139299

Lothenbach, B., Le Saout, G., Gallucci, E., Scrivener, K., 2008. Influence of limestone on the hydration of Portland cements. Cement and Concrete Research 38(6), 848–860. https://doi.org/10.1016/j.cemconres.2008.01.002

Mildner, M., Hotěk, P., Záleská, M., Černý, R., & Fořt, J. (2025). From waste to binder: Alkali activation of blended brick and metakaolin residues for design of circular construction materials. Polymers, 17(20), Article 2720. https://doi.org/10.3390/polym17202720

Pederneiras, C. M., Veiga, R., & de Brito, J. (2021). Physical and mechanical performance of coir fiber-reinforced rendering mortars. Materials, 14(4), 823. https://doi.org/10.3390/ma14040823

Raghunath, S., Hoque, M., & Foster, E. J. (2023). On the roles of cellulose nanocrystals in fiber cement: Implications for rheology, hydration kinetics, and mechanical properties. ACS

Sustainable Chemistry & Engineering, 11(29), 10727–10736. https://doi.org/10.1021/acssuschemeng.3c01392

Razali, N. A. M., Sohaimi, R. M., Othman, R. N. I. R., Abdullah, N., Demon, S. Z. N., Jasmani, L., Yunus, W. M. Z. W., Ya'acob, W. M. H. W., Salleh, E. M., Norizan, M. N., & Halim, N. A. (2022). Comparative study on extraction of cellulose fiber from rice straw waste from the chemo-mechanical and pulping methods. Polymers, 14(3), 387. https://doi.org/10.3390/polym14030387

Sanchez-Echeverri, L. A., Medina-Perilla, J. A., & Ganjian, E. (2020). Nonconventional $Ca(OH)_2$ treatment of bamboo for the reinforcement of cement composites. Materials, 13(8), 1892. https://doi.org/10.3390/ma13081892

Sekar, A., & Kandasamy, G. (2018). Optimization of coconut fiber in coconut shell concrete and its mechanical and bond properties. Materials, 11(9), 1726. https://doi.org/10.3390/ma11091726

Scrivener, K., Snellings, R., Lothenbach, B. (Eds.), 2016. A Practical Guide to Microstructural Analysis of Cementitious Materials. CRC Press, Boca Raton.

Tolêdo Filho, R.D., Scrivener, K., England, G.L., Ghavami, K., 2000. Durability of alkali-sensitive sisal and coconut fibers in cement mortar composites. Cement and Concrete Composites 22(2), 127–143. https://doi.org/10.1016/S0958-9465(99)00039-6

Vagestan, P. K., Periyasamy, M., & Vasugi, V. (2025). Applications of bamboo fiber and bamboo stem ash with styrene butadiene rubber in cement mortar for sustainable structural applications. Scientific Reports, 15, Article 27879. https://doi.org/10.1038/s41598-025-09337-9

Wang, X., Liu, Z., Wang, Y., Zhang, X., & Jiang, M. (2025). Impact behavior of recycled aggregate concrete modified with nano-silica and fibers. Scientific Reports, 15, 19137. https://doi.org/10.1038/s41598-025-04264-1

Wei, X., Yu, J., Dai, G., Liu, L., & Dou, L. (2022). Fiber for recycled aggregate concrete reinforcement: A review. The Journal of the Textile Institute, 114(10), 1573–1580. https://doi.org/10.1080/00405000.2022.2131316

Xiao, J., Yu, C., Wang, B., Duan, Z., & Ma, Z. (2026). Recycled aggregate concrete: Design, application, and challenges. Nature Reviews Clean Technology, 2, 67–83. https://doi.org/10.1038/s44359-025-00125-2

Xu, B., Tian, R., Wang, Y., Zhang, Z.-w., & Zhang, Z. (2024). Preparation and properties of natural bamboo fiber-reinforced recycled aggregate concrete. Materials, 17(12), 2972. https://doi.org/10.3390/ma17122972

Zhang, Y., Wang, Z., Zhang, W., & Ma, H. (2022). A review of recycled aggregate concrete modified by nanosilica and graphene oxide. Journal of Cleaner Production, 375, 134116. https://doi.org/10.1016/j.jclepro.2022.134116

Zhang, Z., Yan, Y., & Geng, G. (2025). A review of micro-resolved crystochemical and mechanical probes for sustainable cement-based material studies. npj Materials Sustainability, 3(1), Article 1. https://doi.org/10.1038/s44296-024-00044-6

Zormati, S., Mhiri, H., Aloulou, F., & Bouaziz, J. (2023). Treatments of nanofiber cellulose biomass for cementitious building materials. Euro-Mediterranean Journal for Environmental Integration, 8, 15–28. https://doi.org/10.1007/s41207-023-00350-w

Zunino, F., Scrivener, K., 2020. The study examines the reaction between metakaolin and limestone, focusing on its effects on porosity refinement and mechanical properties. Cement and Concrete Research 140, 106307. https://doi.org/10.1016/j.cemconres.2020.106307